Estimating the Area, Timing and Duration of Rice Fallows for Agricultural Intensification in India

A pilot study for developing geospatial datasets and improved algorithms for near-real time applications

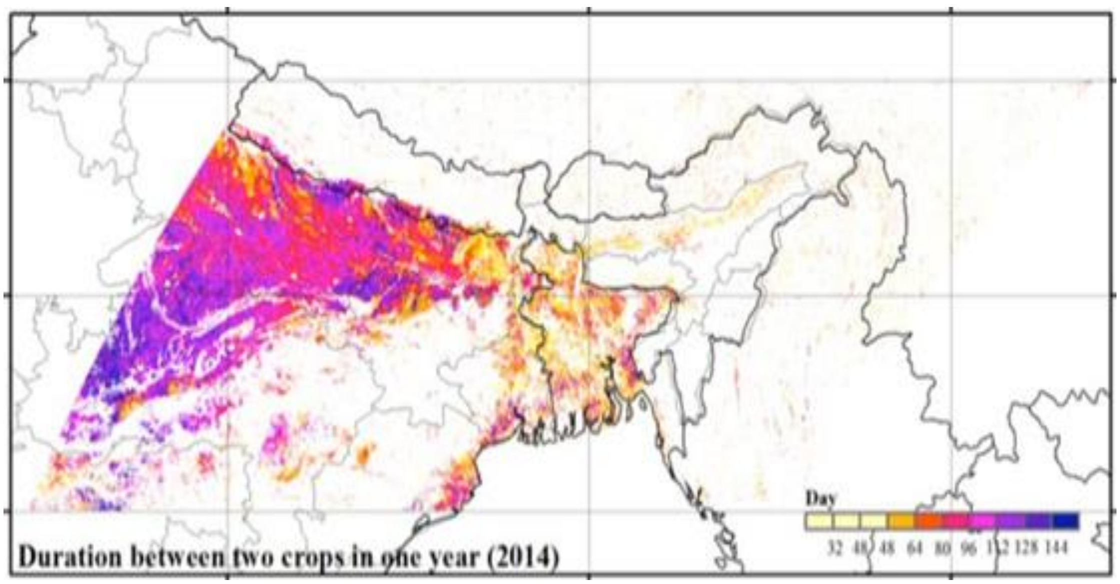

Interim Report

June 2015

Estimating the area, timing and duration of rice fallows for agricultural intensification in India: A pilot study for developing geospatial datasets and improved algorithms

I. Introduction

Agricultural intensification and crop diversification are essential in order to meet the rising demands for food production and security in India, driven by increasing populations and changing food consumption. Fallowing croplands has been a common agricultural practice and serves to accumulate soil moisture in dry regions (dryland farming), or to control weeds and plant diseases. Recently, rotation of crops is considered an alternative method and preferred to fallowing, due to agricultural intensification (growing another crop during the fallow period) and crop diversification (mainly short duration lentils and oil seeds). Rice croplands is widely distributed in India, however, there is no geospatial datasets (maps) about the area, timing and duration of fallowing rice croplands in India. Therefore, there is a need to develop satellite-based technologies that estimate the area, timing and duration of fallowing rice croplands in India. The resultant information can be used to support those studies that assess the potential of agricultural intensification and crop diversification (cultivating short-duration crops) in the fallowing rice croplands.

The long-term and overall goal is to map rice fallows (area and spatial distribution) and to assess feasibility for cropping intensification in rice fallow areas. In this pilot and short-term project, the specific objectives are the followings:

- **Develop algorithms to map cropping intensity and crop fallows using MODIS data during 2000 – 2014 (250-m, 500-m and 1000-m spatial resolution, 8-day temporal resolution).**
- **Develop algorithms to map rice fallow areas at selected sites (Landsat image path/row) in India, using Landsat images during 2000-2014 (30-m spatial resolution, 16-day temporal resolution).**
- **Develop feasibility plans for crop intensification and diversification in rice fallow areas.**

The main purpose of the proposed pilot study is to **map rice fallows and identify potential areas (fallow hotspots) for agricultural intensification (growing another crop during fallow period) and crop diversification (legume and oil seeds)** at the pilot test sites covering a few districts in West Bengal and Odisha (Orissa) to demonstrate technology for large-scale assessment. This case study is to develop operational algorithm to map rice fallows and feasibility analysis at the pilot study for crop intensification and crop diversification in the rice fallow areas. The resultant datasets and algorithms from the pilot study could be applied to large area mapping. This consultant project in satellite remote sensing will also contribute to the CRP Drylands Systems on innovative tools and technology for monitoring and mapping agro-ecosystems at field and landscape scales.

II. Materials and Methods

II.1. Study Areas of the Pilot Study

India is a country with extensive and diverse agriculture, and major crops include paddy rice, wheat, maize and soybean crops. We carried out the pilot study using satellite images from two sensors such as MODIS and Landsat. As these sensors have different spatial resolutions, we selected our pilot study area in the state of West Bengal and Orissa (Odisha).

When MODIS image data are used, the pilot study area covers an area of 20-degree longitude and 10-degree latitude as the case study area, for example, the area covered by MODIS H25V06 and H26V06 tiles, which covers parts of north and eastern India (e.g., Orissa, west Bengal).

When Landsat image data are used, the pilot study area covers dozen of representative districts in the state of West Bengal (Bardawan, Birbhum, Bankura, South 24-Pargana, Purulia, West Mednapur) and Odissa (Balasore, Bhadrak, Kendrapada, Jagatsinghpur and Puri). Specifically, we acquired Landsat images from 2000-2013 for the path/row P139/R044.

Figure 1. A schematic graph to show Landsat path/row in the state of West Bengal and Orissa, India

II.2 Image data from MODIS sensors

II.2.1. Land surface temperature data (MYD11A2)

The MODIS Land Science Team provides 8-day composite MODIS land surface temperature & emissivity products at 1-km resolution, such as MOD11A2 (from the Terra satellite) and MYD11A2 (from the Aqua satellite). The land surface temperature (LST) data include daytime (local time ~10:30am from Terra and ~13:30pm from Aqua) and nighttime (~10:30pm from Terra and ~1:30am from Aqua) temperature observations.

In this study, MYD11A2 data during 2003-2014 were downloaded from the USGS EROS Data Center (https://lpdaac.usgs.gov/). The digital number values (DN) from MYD11A2 were converted to LST with centigrade unit values based on the following formula: LST (°C) = DN × 0.02 – 273.15 (Wan 2008; Wan et al. 2002). The LST data with bad observations in a time series were gap-filled using the linear interpolation approach (Equation 1).

$$VI_{(t+j-1)} = VI_{(t-1)} + j/(n+1) \times (VI_{(t+n)} - VI_{(t-1)}) \quad \ldots\ldots\ldots\ldots\ldots\ldots\ldots\ldots \text{(1)}$$

where $T_{(t+j\text{-}1)}$ is the LST to be interpolated, t is the index of the first bad-quality observation of the n continuous bad observations ($n \leq 3$), j is the order of the bad-quality observation from 1 to n, and t-1 and t+n are the indices of the reliable observations before the first bad-quality observation and after the last bad-quality observation, respectively. We did not interpolate bad-quality observations if they occurred at the beginning and ending 8-day composites in a year.

<u>Deliverable products</u>: (1) daytime LST datasets in 2010 - 2014, and (2) nighttime LST datasets in 2000 – 2014.

II.2.2. Surface reflectance data (MOD09A1)

The MODIS Land Science Team provides an 8-day composite MODIS Surface Reflectance Product at 500-m spatial resolution, such as MOD09A1 from the Terra satellite (Vermote and Vermeulen 1999). It includes seven bands: bands 1 (red: 620-670 nm), 2 (near infrared 1: 841-876 nm), 3 (blue: 459-479 nm), 4 (green: 545-565 nm), 5 (near infrared 2: 1230-1250 nm), 6 (shortwave infrared 1: 1628-1652 nm), and 7 (shortwave infrared 2: 2105-215 nm).

Standard MODIS products are organized in a tile system using a sinusoidal projection, and each tile covers an area of 1,200 km × 1,200 km (approximately 10° latitude by 10°longitude at the equator). Our study area is covered within two tiles (H25V06 and H26V06) of MOD09A1 data. We downloaded these two tiles for 2000-2014 (46 composites per year) from the USGS EROS Data Center (https://lpdaac.usgs.gov/).

Our MODIS preprocessing procedure included three components: (1) clouds and cloud shadows, (2) calculation of spectral indices, and (3) gap-filling of vegetation indices.

We identified cloud cover and cloud shadows in two steps. First, we used the data quality information (the quality control flag layer) in the MOD09A1 products to extract the clouds from each image. Second, we applied an additional restriction in which pixels with a blue reflectance of ≥ 0.2 were also labeled as cloudy. Therefore, 46 maps of cloud cover were generated. For each pixel, any 8-day composite that was identified as cloud cover was excluded from further analyses. Figure 2 shows numbers of good-quality observations in 2014 over the study area in India.

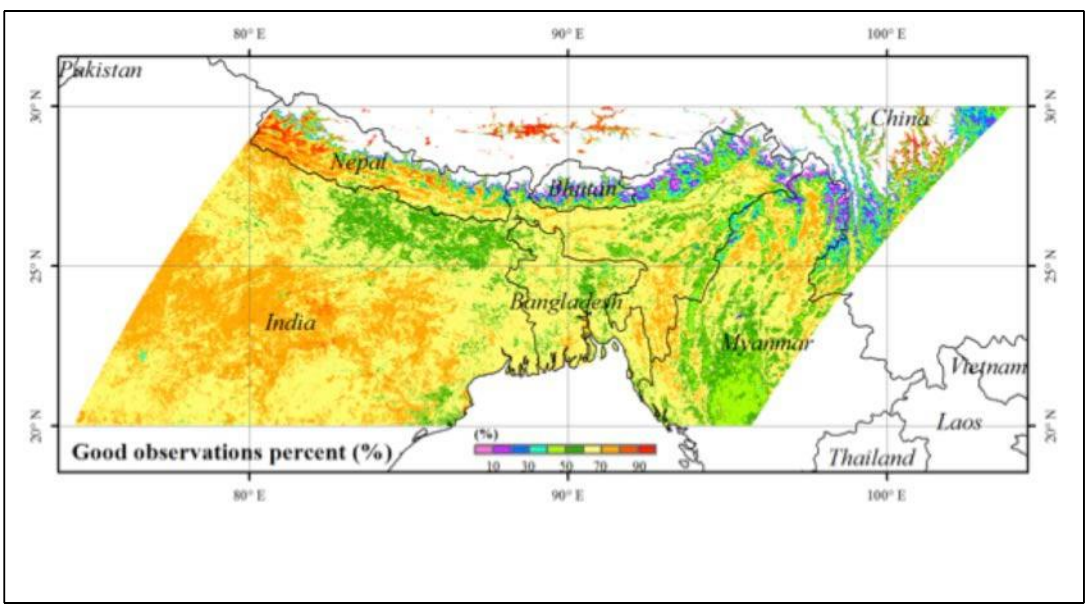

Figure 2. The map of frequency (numbers) of good-quality observations (8-day composites) in 2014 in India.

The individual spectral bands in each of the 8-day composite surface reflectance MOD09A1 datasets were used to calculate four spectral indices: (1) Normalized Difference Vegetation Index (NDVI), (2) Enhanced Vegetation Index (EVI), (3) Land Surface Water Index (LSWI), and (4) Normalized Difference Snow Index (NDSI) (see Equations 2 - 5):

$$NDVI = \frac{\rho_{nir} - \rho_{red}}{\rho_{nir} + \rho_{red}} \quad (2)$$

$$LSWI = \frac{\rho_{nir} - \rho_{swir}}{\rho_{nir} + \rho_{swir}} \quad (3)$$

$$EVI = 2.5 \times \frac{\rho_{nir} - \rho_{red}}{\rho_{nir} + 6 \times \rho_{red} - 7.5 \times \rho_{blue} + 1} \quad (4)$$

$$NDSI = \frac{\rho_{green} - \rho_{nir}}{\rho_{green} + \rho_{nir}} \quad (5)$$

where ρ_{blue}, ρ_{green}, ρ_{red}, ρ_{nir} and ρ_{swir} are the reflectance for the blue (Band 3), green (Band 4), red (Band 1), NIR (Band 2), and SWIR (Band 6, shortwave infrared 1) bands, respectively. Both NDVI and EVI are related to the vegetation canopy. NDVI has a saturation issue when it is used for closed canopies, and it is also sensitive to atmospheric conditions and soil background (Huete et al. 2002; Xiao et al. 2003). EVI accounts for residual atmospheric contamination and variable soil and canopy background reflectance (Huete et al. 2002; Huete et al. 1997) because the blue band is sensitive to atmospheric conditions. LSWI was shown to be sensitive to equivalent water thickness (EWT; g H_2O/m^2) (Maki et al. 2004; Xiao et al. 2002a, b) because the SWIR band is sensitive to leaf water and soil moisture. NDSI is widely used for snow detection (Hall et al. 1995; Hall et al. 2002).

Deliverable products: (1) 8-day surface reflectance data during 2000 – 2014, and (2) 8-day vegetation indices (NDVI, EVI, LSWI, and NDSI) data during 2000 – 2014

II.3. Image data from Landsat sensors

We downloaded Landsat TM, ETM+ and OLI images in 2000 – 2014 from the USGS EROS data center. Atmospheric correction was applied to these images to generate surface reflectance. We calculated four spectral indices: NDVI, EVI, LSWI and NDSI for each of the images.

III. Results and Discussion

III.1. Temperature-defined crop growing seasons, based on land surface temperature

Air temperature and land surface temperature are important climatic variables that determine planting date, harvesting date and duration (length) of crop growing season. Where does temperature constrain crop cultivation in India? As there are a limited number of weather

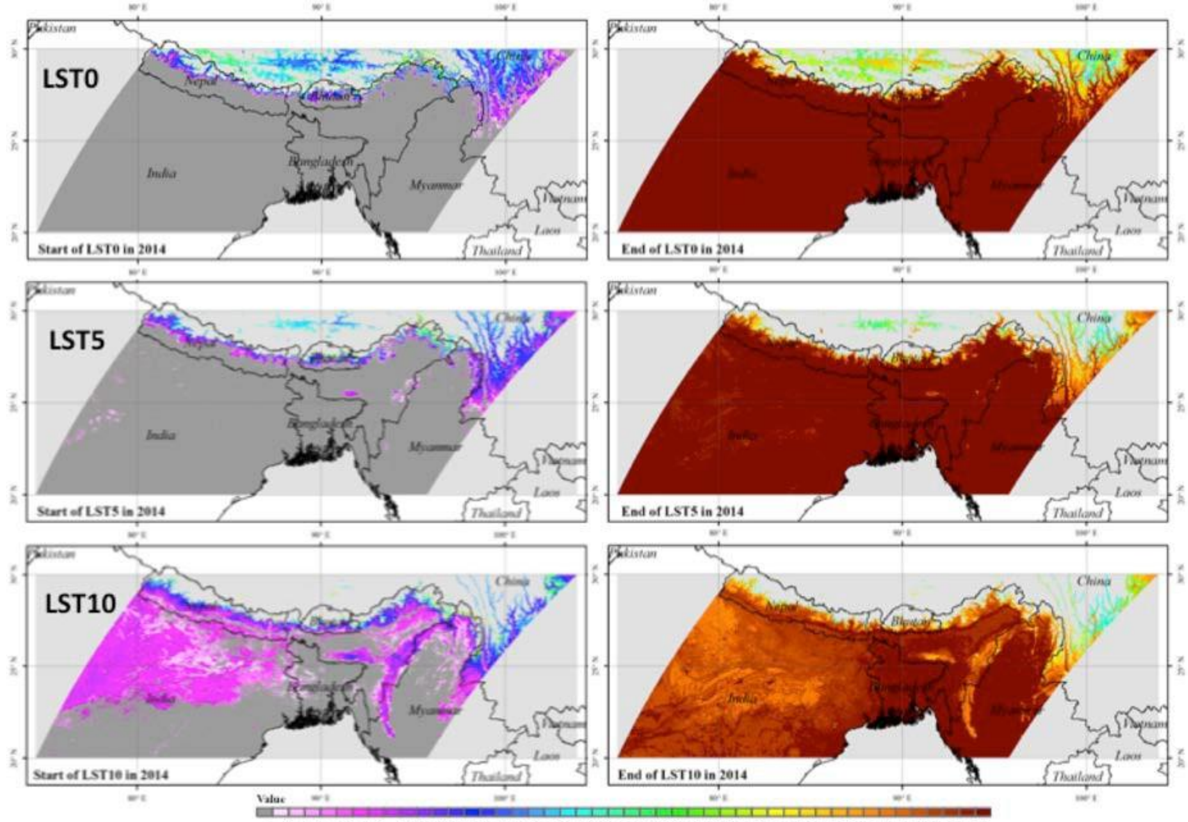

Figure 3. Starting date, ending date and duration of the plant growing season in 2010, as defined by the nighttime LST > 5 ^oC.

stations in India, there are very limited amounts of air temperature data in India. In comparison, MODIS-based LST data provide continuous spatial and temporal coverage in India, and make it possible to generate maps of crop growing seasons as defined by LST. Here we use nighttime LST > 0, 5, and 10 ^{o}C as threshold values to generate maps of starting dates in spring, ending dates in fall, and duration (length) of plant growing seasons. Considering the variation of LST retrieval, we assume 3 consecutive 8-day composites to meet the criterion of LST > 0, 5 and 10 ^{o}C. Figure 3 shows the spatial distributions of starting date and ending date of plant growing season as defined by the nighttime LST > 0, 5 and 10 ^{o}C. It suggests that temperature does not constrain crop cultivation in most of India.

Deliverable products: (1) maps of plant growing seasons in 2000-2014, based on LST > 0 ^{o}C, which is appropriate for natural grasses, shrubs and trees; (2) maps of crop growing season in 2000 – 2014, based on LST > 5 ^{o}C, which is appropriate for some crops such as winter wheat; and (3) maps of crop growing season in 2000 – 2014, based LST > 10 ^{o}C, which is appropriate for some summer crops.

III.2. Map of cropping intensity (single and double cropping in a year) in 2014

Vegetation canopies can be described by leaf area index (LAI), pigment concentration (e.g., chlorophyll content) and leaf/canopy water content. It is well known that NDVI is related to LAI, EVI is related to leaf/canopy chlorophyll content, and LSWI is related to leaf/canopy water content (Xiao et al., 2006). As shown in Figure 3, there are strong seasonal dynamics of vegetation indices in croplands over time.

We analyzed NDVI, EVI and LSWI and used several metrics to describe the seasonality of

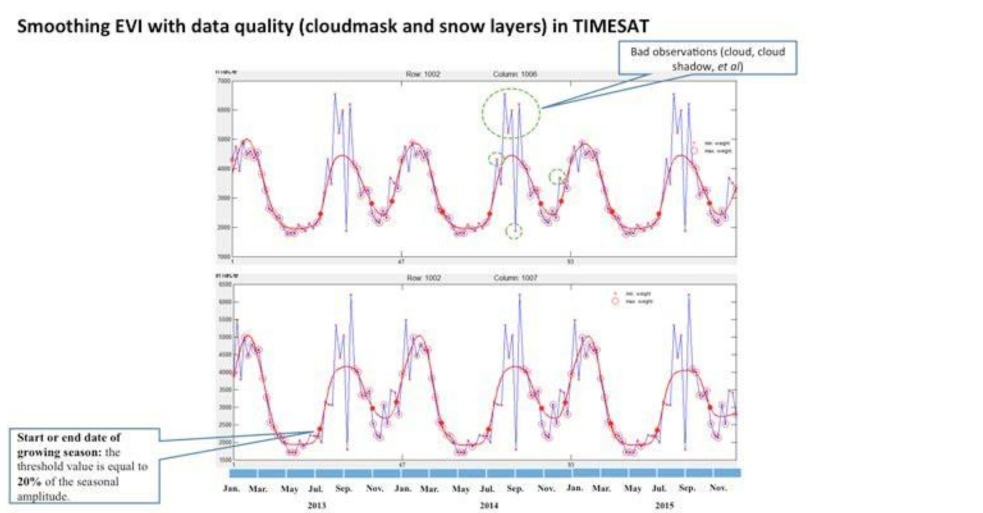

Figure 4. Seasonal dynamics of EVI in a MODIS pixel.

vegetation indices over the period of 2000 - 2014. Seasonal dynamics of EVI illustrates clearly two crops in a year over a MODIS pixel (Figure 4). We applied the TIMESAT software to EVI time series data and generated a map of cropping intensity in 2014 (Figure 5).

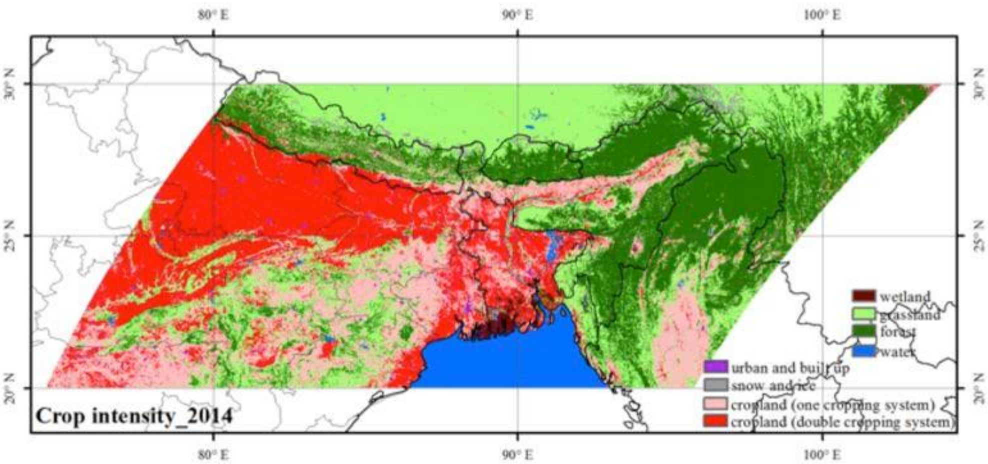

Figure 5. The map of cropping intensity in India in 2014, as generated from analysis of MODIS data.

Deliverable products: map of the cropping intensity in India in 2014.

III.3. Map of starting date, ending date and duration of crop fallow in 2014

The seasonal dynamics of vegetation indices also illustrate well the starting date, ending date and duration of crop fallow in a MODIS pixel (Figure 3). We applied the TIMESAT to the EVI time series data of individual pixels and then generated maps of starting date and ending date of crop fallow in 2014 (Figure 6), and then the duration of crop fallow in 2014 at individual pixels (Figure 7).

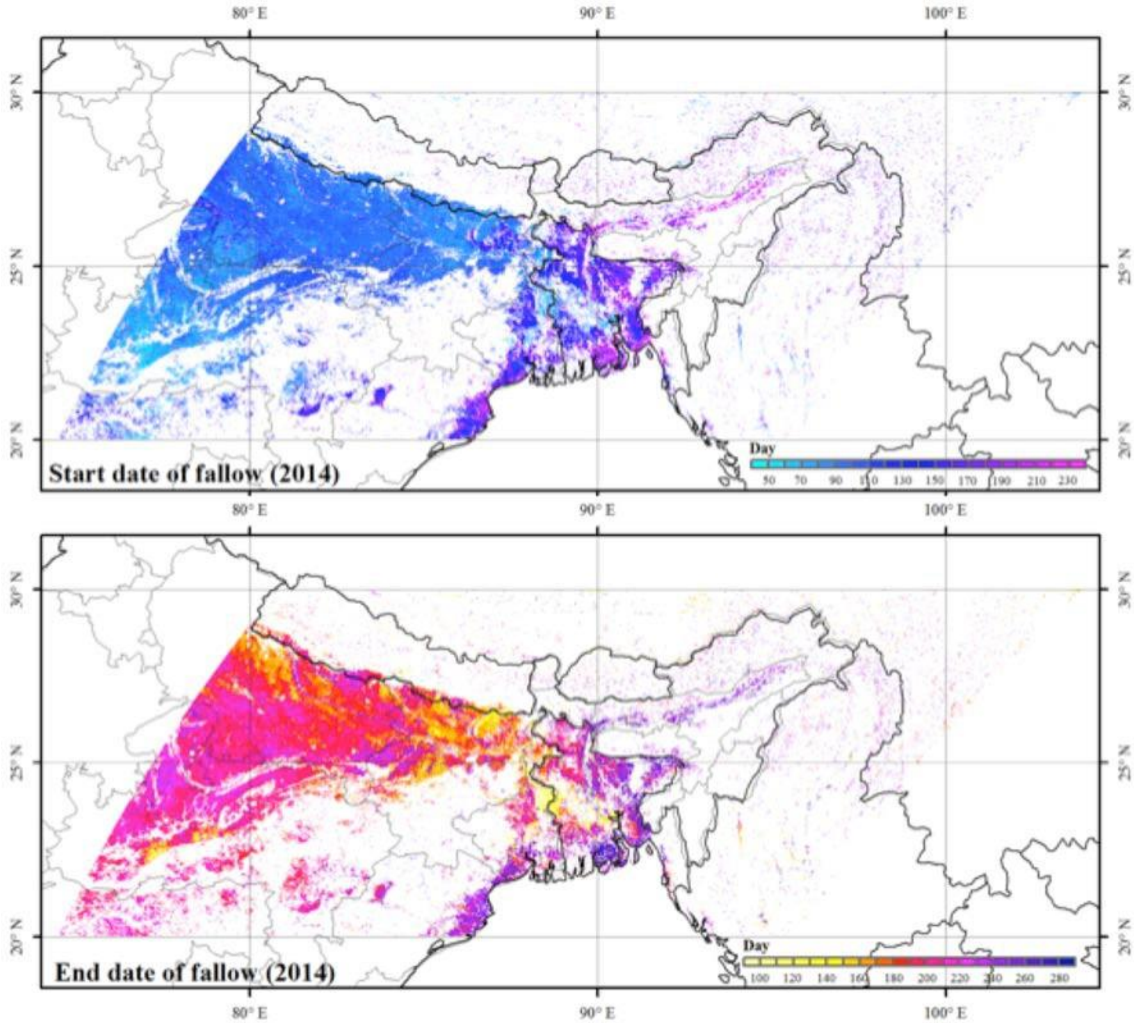

Figure 6. The starting date and ending date of crop fallows in India in 2014 at individual MODIS pixels.

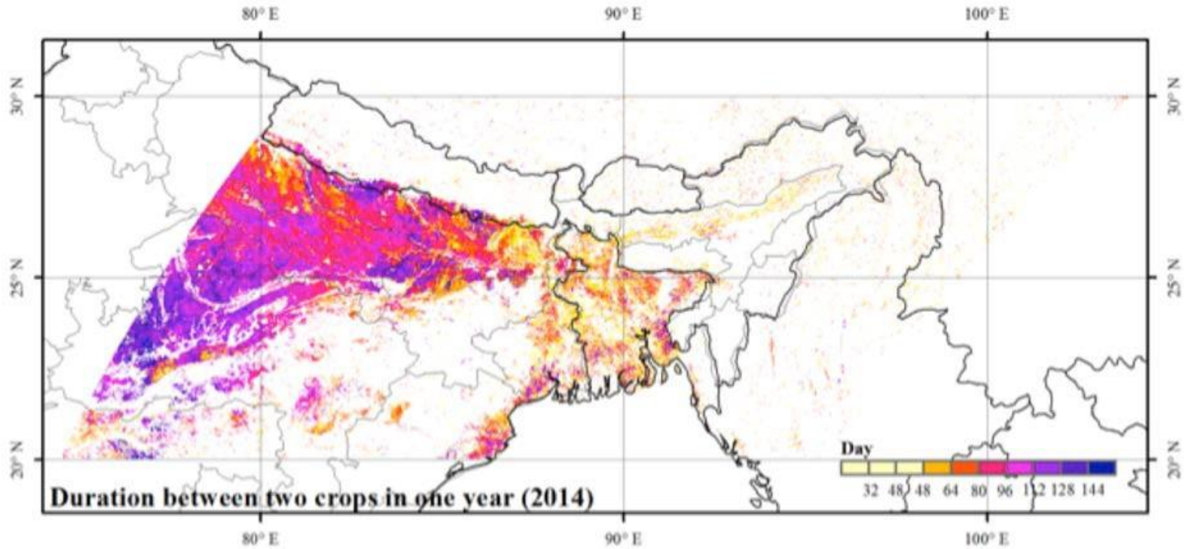

Figure 7. The duration of crop fallows in India in 2014 at individual MODIS pixels

III.4. Map of crop fallow area in 2014 from Landsat images

We conducted visual interpretation of individual Landsat images through various band composites and carried out exploratory data analysis for individual image within the period of cropland fallow in 2014. The visual interpretation results show that Landsat image in 12/2014 clearly illustrates where crop fallow area in 2014 at 30-m spatial resolution.

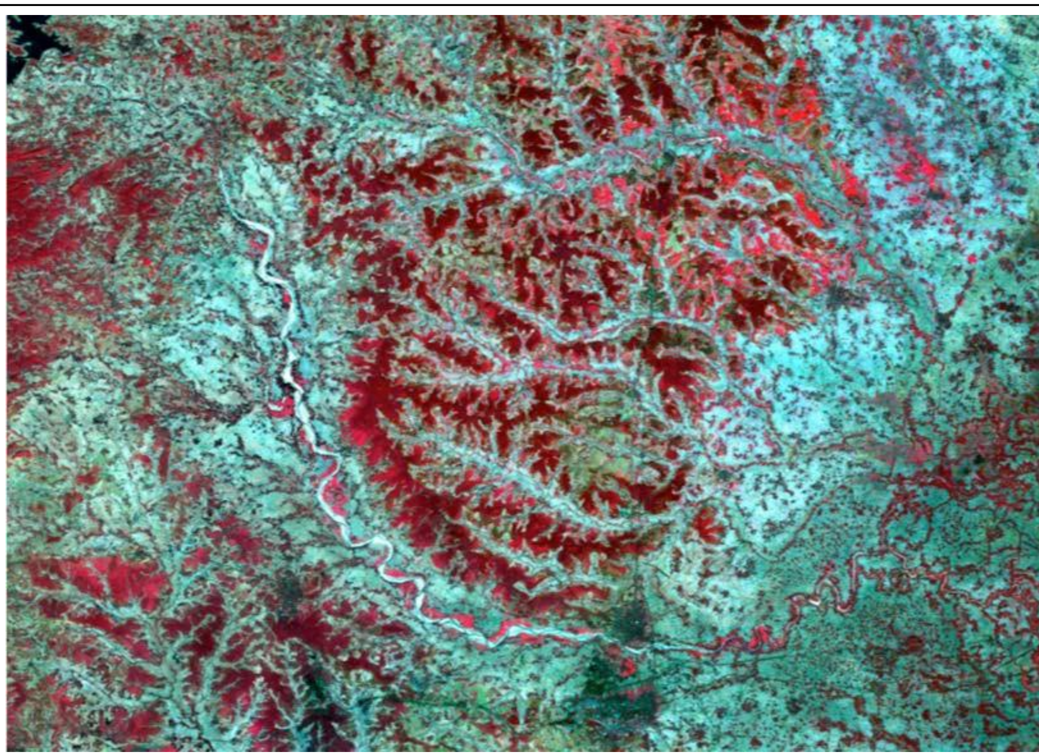

Figure 8. The false color composite of Landsat images in 12/2014. The cyan color clearly illustrates fallowed croplands.

IV. Summary (interim)

In this pilot study, we analyzed the seasonal dynamics of three vegetation indices (NDVI, EVI and LSWI) in the study area from MODIS sensors. We used the TIMESAT software and EVI time series data in 2014 to generate (1) map of cropping intensity, (2) maps of starting date, ending date and duration of crop fallows in 2014 at 500-m spatial resolution. The resultant maps need to be further evaluated through in-situ data collected by the researchers in the study area. Such evaluation task is beyond the scope of this pilot study, and we expect that it will be incorporated into the future study.

In this pilot study, we also analyzed Landsat images acquired within the period of crop fallow as defined by the MODIS time series data. Visual interpretation of Landsat images in 2014 shows that crop fallow at 30-m spatial resolution (Landsat) is a dynamic process, and reaches its large area in December 2014. This suggests that through integration of MODIS time series data analysis and Landsat multi-temporal image analysis, it is possible to characterize crop fallow in India at 500-m and 30-m spatial resolution.

Based on the results and lessons from this pilot study, our recommendation is that there is a need to explore MODIS data at 250-m and 500-m spatial resolutions to better define cropping intensity, starting date (planting date), ending date (harvesting date) and duration of crop fallow in India. India has diverse and extensive crop cultivation, and cropland field size distribution is dominated with small farms, therefore, it remains a challenging task to track and monitor cropland dynamics. Second recommendation is that detail study need to conducted with incorporating optical as well microware remote sensing data along with extensive in-situ observation to improve the algorithms and overcome the cloud cover during the monsoon season.

First phase of the study is in progress, next phases of the study involves conducting analysis at higher spatial scales and develop feasibility plan for specific crops and crop varieties.

Reference

Berger, J., Buuveibaatar, B., & Mishra, C. (2013). Globalization of the Cashmere Market and the
Decline of Large Mammals in Central Asia. *Conservation Biology, 27*, 679-689

Chuluun, T., & Ojima, D. (2002). Land use change and carbon cycle in and and semi-arid lands of East and Central Asia. *Science in China Series C-Life Sciences, 45*, 48-+

Emerson, C., Veeck, G., Li, Z., Yu, F.W., & Zhang, H.P. (2010). Biophysical and Agroeconomic
Influences on Pasture Quality in Da'erhanmaoming'an Union Banner, Inner Mongolian Autonomous Region, China. *Physical Geography, 31*, 552-581

Hall, D.K., Riggs, G.A., & Salomonson, V.V. (1995). Development of Methods for Mapping Global Snow Cover Using Moderate Resolution Imaging Spectroradiometer Data. *Remote Sensing of Environment, 54*, 127-140

Hall, D.K., Riggs, G.A., Salomonson, V.V., DiGirolamo, N.E., & Bayr, K.J. (2002). MODIS snow-cover products. *Remote Sensing of Environment, 83*, 181-194

Huete, A., Didan, K., Miura, T., Rodriguez, E.P., Gao, X., & Ferreira, L.G. (2002). Overview of the radiometric and biophysical performance of the MODIS vegetation indices. *Remote Sensing of Environment, 83*, 195-213

Huete, A.R., Liu, H.Q., Batchily, K., & vanLeeuwen, W. (1997). A comparison of vegetation indices global set of TM images for EOS-MODIS. *Remote Sensing of Environment, 59,* 440-451

John, R., Chen, J.Q., Noormets, A., Xiao, X.M., Xu, J.Y., Lu, N., & Chen, S.P. (2013). Modelling gross primary production in semi-arid Inner Mongolia using MODIS imagery and eddy covariance data. *International Journal of Remote Sensing, 34,* 2829-2857

Kalfas, J.L., Xiao, X., Vanegas, D.X., Verma, S.B., & Suyker, A.E. (2011). Modeling gross primary production of irrigated and rain-fed maize using MODIS imagery and CO< sub> 2</sub> flux tower data. *Agricultural and Forest Meteorology, 151,* 1514-1528

Kariyeva, J., & van Leeuwen, W.J.D. (2011). Environmental Drivers of NDVI-Based Vegetation Phenology in Central Asia. *Remote Sensing, 3,* 203-246

Li, H.W., & Yang, X.P. (2014). Temperate dryland vegetation changes under a warming climate and strong human intervention - With a particular reference to the district Xilin Gol, Inner Mongolia, China. *Catena, 119,* 9-20

Li, Z., Yu, G., Xiao, X., Li, Y., Zhao, X., Ren, C., Zhang, L., & Fu, Y. (2007). Modeling gross primary production of alpine ecosystems in the Tibetan Plateau using MODIS images and climate data. *Remote Sensing of Environment, 107,* 510-519

Maki, M., Ishiahra, M., & Tamura, M. (2004). Estimation of leaf water status to monitor the risk of forest fires by using remotely sensed data. *Remote Sensing of Environment, 90,* 441-450

Sternberg, T., Tsolmon, R., Middleton, N., & Thomas, D. (2011). Tracking desertification on the Mongolian steppe through NDVI and field-survey data. *International Journal of Digital Earth, 4,* 50-64

Vermote, E., & Vermeulen, A. (1999). Atmospheric correction algorithm: spectral reflectances (MOD09). *ATBD version, 4*

von Wehrden, H., Hanspach, J., Ronnenberg, K., & Wesche, K. (2010). Inter-annual rainfall variability in Central Asia - A contribution to the discussion on the importance of environmental stochasticity in drylands. *Journal of Arid Environments, 74,* 1212-1215

Wagle, P., Xiao, X.M., Torn, M.S., Cook, D.R., Matamala, R., Fischer, M.L., Jin, C., Dong, J.W., & Biradar, C. (2014). Sensitivity of vegetation indices and gross primary production of tallgrass prairie to severe drought. *Remote Sensing of Environment, 152,* 1-14

Wan, Z.M. (2008). New refinements and validation of the MODIS Land-Surface Temperature/Emissivity products. *Remote Sensing of Environment, 112,* 59-74

Wan, Z.M., Zhang, Y.L., Zhang, Q.C., & Li, Z.L. (2002). Validation of the land-surface temperature products retrieved from Terra Moderate Resolution Imaging Spectroradiometer data. *Remote Sensing of Environment, 83,* 163-180

Wang, Y., Roderick, M.L., Shen, Y., & Sun, F. (2014). Attribution of satellite-observed vegetation trends in a hyper-arid region of the Heihe River basin, Western China. *Hydrology and Earth System Sciences, 18,* 3499-3509

Wang, Z., Xiao, X., & Yan, X. (2010a). Modeling gross primary production of maize cropland and degraded grassland in northeastern China. *Agricultural and Forest Meteorology, 150,* 1160-1167

Wang, Z., Xiao, X.M., & Yan, X.D. (2010b). Modeling gross primary production of maize cropland and degraded grassland in northeastern China. *Agricultural and Forest Meteorology, 150,* 1160-1167

Wu, W., Wang, S., Xiao, X., Yu, G., Fu, Y., & Hao, Y. (2008). Modeling gross primary

production of a temperate grassland ecosystem in Inner Mongolia, China, using MODIS imagery and climate data. *Science in China Series D: Earth Sciences*, *51*, 1501-1512
Xiao, X., Boles, S., Frolking, S., Salas, W., Moore, B., Li, C., He, L., & Zhao, R. (2002a). Landscape-scale characterization of cropland in China using Vegetation and Landsat TM images.
International Journal of Remote Sensing, *23*, 3579-3594
Xiao, X., Boles, S., Frolking, S., Salas, W., Moore, B., Li, C., He, L., & Zhao, R. (2002b). Observation of flooding and rice transplanting of paddy rice fields at the site to landscape scales in China using VEGETATION sensor data. *International Journal of Remote Sensing*, *23*, 3009-
3022
Xiao, X., Hollinger, D., Aber, J., Goltz, M., Davidson, E.A., Zhang, Q., & Moore Iii, B. (2004a). Satellite-based modeling of gross primary production in an evergreen needleleaf forest. *Remote Sensing of Environment*, *89*, 519-534
Xiao, X., Zhang, Q., Braswell, B., Urbanski, S., Boles, S., Wofsy, S., Moore III, B., & Ojima, D.
(2004b). Modeling gross primary production of temperate deciduous broadleaf forest using satellite images and climate data. *Remote Sensing of Environment*, *91*, 256-270
Xiao, X., Zhang, Q., Hollinger, D., Aber, J., & Moore III, B. (2005a). Modeling gross primary production of an evergreen needleleaf forest using MODIS and climate data. *Ecological*
Applications, *15*, 954-969
Xiao, X., Zhang, Q., Saleska, S., Hutyra, L., De Camargo, P., Wofsy, S., Frolking, S., Boles, S., Keller, M., & Moore III, B. (2005b). Satellite-based modeling of gross primary production in a seasonally moist tropical evergreen forest. *Remote Sensing of Environment*, *94*, 105-122
Xiao, X.M., Braswell, B., Zhang, Q.Y., Boles, S., Frolking, S., & Moore, B. (2003). Sensitivity of vegetation indices to atmospheric aerosols: continental-scale observations in Northern Asia.
Remote Sensing of Environment, *84*, 385-392